IMA Journal of Applied Mathematics (2016) Page 1 of 19
doi:10.1093/imamat/xxx000

Asymptotic analysis of a Bragg fiber: a multiple scales approach

B. MALING & R. V. CRASTER
Department of Mathematics, Imperial College London, London SW7 2AZ, UK

[Received on 16 August 2016]

We develop an asymptotic approach to find the guided modes, and their frequencies, within a Bragg fiber consisting of a cylindrical dielectric core surrounded by concentric cylindrical cladding layers; these fibers have the aim of transporting electromagnetic waves over long distances with minimal transmission losses. We derive a scalar ordinary differential equation eigenvalue problem on a dynamic long-scale that has the details of the short-scale field built into its coefficients, which is then straightforward to solve. The resulting asymptotic results are compared against full numerical solutions and their accuracy verified.

Keywords:

Homogenisation; electromagnetic waves; periodic structures

1. Introduction

It is well known that a periodic stack of alternating dielectric materials exhibits photonic band gaps, forbidding the propagation of electromagnetic waves at certain frequencies. The resulting structure is employed in different contexts, i.e. as a Bragg mirror or grating (Fink et al., 1998; Chigrin et al., 1999), which have practical applications as optical filters in lasers (Volodin et al., 2004), in laser transmission with low losses (Temelkuran et al., 2002) and elsewhere. As was first noted in 1978 (Yeh et al., 1978), if the same layered structure is wrapped around a cylindrical core, the band gap effect can be used to confine electromagnetic radiation resulting in an optical fiber that works by a fundamentally different principle to that of a conventional fiber, allowing for a higher degree of confinement, as well as the interesting possibility of low-index or hollow core fibers. Since then, these so-called Bragg fibers have been fabricated experimentally (Fink et al., 1999), and there has been much further development in the theory of microstructured optical fibers (Russell, 2003) such as photonic crystal fibers (PCFs) (Zolla et al., 2005; Joannopoulos et al., 2008). Nonetheless the Bragg fiber remains of considerable interest due to its feasibility of fabrication, low transmission losses, and the possibility of single-mode transmission.

The analysis of planar Bragg gratings/reflectors is straightforward (Yeh et al., 1977) using transfer matrix methods (Markos & Soukoulis, 2008), as the problem is essentially one-dimensional. The mathematical analysis of Bragg fibers is not so straightforward and is complicated by two factors; firstly, the repeating layer arrangements are no longer strictly periodic due to their curvature, and hence the electromagnetic fields do not satisfy the conditions for Bloch's theorem to be applied. Secondly, guided modes can no longer necessarily be separated into scalar transverse electric (TE) or transverse magnetic (TM) modes, and hence a fully coupled treatment of Maxwell's equations is necessary. Fully numerical treatments based upon finite element method (FEM) simulations (Joannopoulos et al., 2011), finite differences (Mizrahi & Schächter, 2004; Wu et al., 2005), or other methods are possible and we utilise FEM software (Comsol® 5.0) later for comparative purposes, but these do not provide insight or give rapid solutions. Proceeding analytically instead, an eigenvalue problem for the guided modes emerges and it is necessary either to treat each cladding layer individually, as in Yeh et al. (1978), which leads to

© The author 2016. Published by Oxford University Press on behalf of the Institute of Mathematics and its Applications. All rights reserved.

a cumbersome matrix eigenvalue problem involving potential ill-conditioning from the Bessel functions within the matrix, or alternatively to make an asymptotic approximation of some sort within the transfer matrix methodology that underlies the problem setup. In Xu et al. (2000), asymptotic expressions for the Bessel functions $\mathrm{J}_\nu(x)$ and $\mathrm{Y}_\nu(x)$ as $x \to \infty$ are used and in doing so, a much simpler eigenvalue problem is posed, and for a typical set of parameters, the resulting eigenvalues are shown to be within 2% of those of the original problem. The limitation of this approach is that the asymptotic approximation requires the core radius of the fiber to be significantly larger than the reciprocal of the radiation's transverse wave vector. In Xu et al. (2002), the methodology is developed further, and it is shown that by treating a small number of inner layers exactly, and the remaining layers asymptotically, the eigenvalues can be found accurately even for small-core fibers.

In this article we develop a complementary alternative method, based on a two-scale asymptotic analysis, which instead requires the core radius to be large compared with the thickness of one of the cladding layers. Since we know from classical Bragg theory (Markos & Soukoulis, 2008) that optimal confinement occurs when the layer thickness is of the order of a quarter-wavelength, the requirements of this vis-a-vis those of Xu et al. (2000) are roughly equivalent. The asymptotic methodology we employ leads to a simple eigenvalue problem for a scalar ordinary differential equation, which encapsulates the details of the layering through integrated quantities, and no matrix analysis is required at all. This approach is based upon the high frequency homogenisation of Craster et al. (2010) and, in effect, the alternating layers surrounding the core are replaced by an effective cladding whose characteristics are defined by a long-scale equation, with the short-scale behaviour encapsulated within its coefficients. As we shall see, the results yielded by our method will have a similar degree of accuracy to those reported in the articles Xu et al. (2000, 2002), with the advantage that we also arrive at a closed-form solution for the radiation decay in the outer layers. As a final comment, the application of a homogenisation approach to a microstructured optical fiber in this article can be viewed as a canonical example; in principle the method could be extended and applied for other types of microstructured optical fibers, the study of which is a very active area of research.

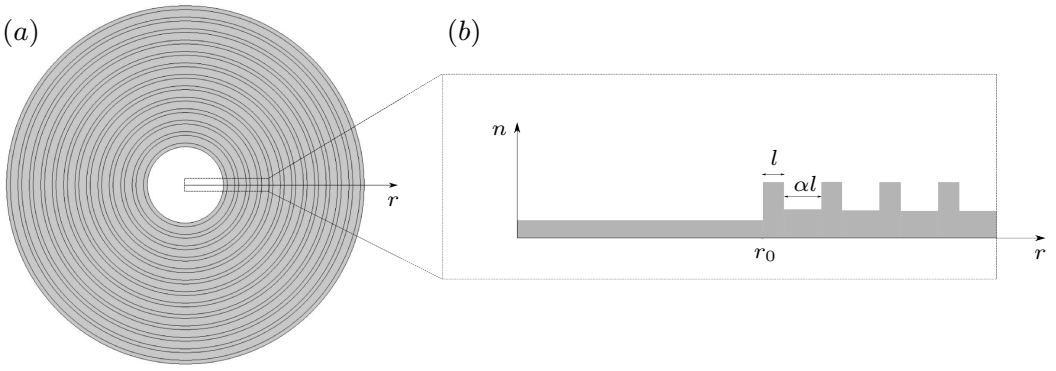


FIG. 1: (a) Cross-section of a Bragg fiber of the type studied in this article. Inset (b) shows the refractive index profile of the core and first 4 pairs of cladding layers. The core has a refractive index n_0, and the alternating layers of thickness l and αl have index n_1 and n_2 respectively.

2. Theory

We consider an optical fiber of the type shown in Fig. 1, consisting of a cylindrical core of radius r_0, which may be hollow or filled, surrounded by a cladding shell formed of alternating concentric layers of two dielectric materials of thickness l and αl, with refractive index n_1 and n_2 respectively. We will assume that the fiber contains a sufficient number of layer pairs that the field decays almost completely before reaching the outer boundary. Mathematically, this allows us to let the number of layer pairs tend to infinity, resulting in a cladding region that is semi-infinite in the radial direction.

2.1 *Governing system*

For a system with cylindrical symmetry that is invariant in the z-direction, Maxwell's equations permit solutions of the form

$$\begin{pmatrix} \mathbf{H}(r,\phi,z,t) \\ \mathbf{E}(r,\phi,z,t) \end{pmatrix} = \begin{pmatrix} \mathbf{H}(r) \\ \mathbf{E}(r) \end{pmatrix} \exp[i(\hat{\beta}z + m\phi - \omega t)], \tag{2.1}$$

where ω is the harmonic frequency, $\hat{\beta}$ is the propagation constant, and $m \in \mathbb{Z}$ is the azimuthal quantum number. The field in each region of the fiber can then be specified completely by the longitudinal components of the magnetic and electric field, which are governed by Bessel-like equations:

$$\left\{ \frac{\mathrm{d}^2}{\mathrm{d}r^2} + \frac{1}{r}\frac{\mathrm{d}}{\mathrm{d}r} + \frac{n^2\omega^2}{c^2} - \hat{\beta}^2 - \frac{m^2}{r^2} \right\} \begin{pmatrix} H_z(r) \\ E_z(r) \end{pmatrix} = 0, \tag{2.2}$$

where $n(r) = \sqrt{\varepsilon(r)}\sqrt{\mu(r)}$ is a piecewise-constant function representing the refractive index profile of the fiber. We note that propagating solutions exist only if $\omega/\hat{\beta} > c/n$, so we assume this is the case in every region of the fiber. The weak form of Maxwell's equations requires continuity of the components of $\mathbf{H}$ and $\mathbf{E}$ tangential to any phase change between media. As noted in Guenneau et al. (2003), these quantities are also naturally written in terms of longitudinal components - in this case leading to the following mixed boundary conditions at each interface between different media:

$$[E_z] = 0, \qquad \left[\frac{\hat{\beta}m}{n^2\omega^2/c^2 - \hat{\beta}^2} \frac{H_z}{r} + \frac{i\varepsilon\omega/c}{n^2\omega^2/c^2 - \hat{\beta}^2} \frac{\partial E_z}{\partial r} \right] = 0. \tag{2.3}$$

$$[H_z] = 0, \qquad \left[\frac{\hat{\beta}m}{n^2\omega^2/c^2 - \hat{\beta}^2} \frac{E_z}{r} - \frac{i\mu\omega/c}{n^2\omega^2/c^2 - \hat{\beta}^2} \frac{\partial H_z}{\partial r} \right] = 0, \tag{2.4}$$

where $[\cdot]$ denotes a jump discontinuity across the interface. We note that for $m = 0$ and/or $\hat{\beta} = 0$, these conditions allow the components of (2.2) to be decoupled, resulting in transverse electric (TE), or transverse magnetic (TM), modes. In particular, the fundamental TE and TM guided modes have $m = 0$, $\hat{\beta} \neq 0$, and are the ones of interest in the design of single-mode fibers (Yeh et al., 1978).

The aim is to find solutions of equation (2.2) for the index profile described in Fig. 1, subject to the boundary conditions (2.3) and (2.4) at each phase interface, and which decay exponentially as $r \to \infty$. Our approach will be to consider the layered cladding region and the uniform core separately; first we apply an asymptotic homogenisation scheme to the layers, resulting in an effective equation that governs the field decay in the region $r > r_0$, and then connect the solution of this to the field in the core region $r < r_0$ using boundary conditions at $r = r_0$.

2.2 *The cladding region*

The confinement of the electromagnetic field to the core region relies on the photonic band-gap effect in the surrounding layers of the fiber. Our aim is to homogenise these surrounding layers such that they can be considered as a single, continuous cladding region, whose properties take into account the layered microstructure. Classical homogenisation theories are valid within the quasi-static regime, in which the wavelength of the radiation is far greater than the characteristic size of the microstructure (see Bakhvalov & Panasenko (1989); Bensoussan et al. (1978); Oleinik et al. (1992); Zhikov et al. (1994) for examples). Clearly, this is not the case in our current problem, as the interference necessary to induce a photonic band gap relies on the wavelength and the microstructure being of comparable size. Instead, we adopt a high-frequency homogenisation (HFH) method based on the one developed in Craster et al. (2010), which instead relies on the harmonic frequency being close to a standing wave eigenfrequency of a periodic structure. Since the band gaps of a periodic structure are bounded by standing wave eigenfrequencies, this regime is appropriate for the present problem. The original article demonstrated that propagating waves in a periodic structure such as a photonic crystal can then be represented by slowly-varying scalar functions that modulate rapidly-oscillating Bloch eigenstates.

In order for the standard HFH methodology to be applied to our problem, it would be necessary for the equations governing the layered structure to permit Bloch wave solutions. In fact, this is not the case for equation (2.2), which reflects the fact that due to the curvature of the layers, the structure is not perfectly periodic. Fortunately, progress can be made if the thickness of the concentric layers is much smaller than the inner radius of the shell, i.e. $l \ll r_0$. Assuming that this is the case, we define a small parameter $\eta = l/r_0$ and assume $\eta \ll 1$ using this as our asymptotic parameter. In the relevant part of the cladding region we then have $l/r = \eta r_0/r$ where $r_0/r = O(1)$.

In order to adopt a two-scale approach, we divide the cladding into repeating cells of two neighbouring layers and define a short-scale radial cell coordinate as $\xi = (r - r_c)/l$, where r_c is the position of the interface between two layers inside the cell, and hence $-1 \leqslant \xi \leqslant \alpha$ in each cell. Alongside this, we define a long-scale radial coordinate $R = \eta r/l$, and treat ξ and R as independent variables. Dropping the z subscript henceforth, we write the longitudinal components of fields as $H(R,\xi), E(R,\xi)$, and expand the operators in (2.2) in two scales using the chain rule to get the following system:

$$\left\{ \frac{\partial^2}{\partial \xi^2} + \left(n_i^2 \Omega^2 - \beta^2\right) + \eta \left(2\frac{\partial^2}{\partial R \partial \xi} + \frac{1}{R}\frac{\partial}{\partial \xi} \right) + \eta^2 \left(\frac{\partial^2}{\partial R^2} + \frac{1}{R}\frac{\partial}{\partial R} - \frac{\xi}{R^2}\frac{\partial}{\partial \xi} - \frac{m}{R^2} \right) \right\} \begin{pmatrix} H(R,\xi) \\ E(R,\xi) \end{pmatrix} = 0. \tag{2.5}$$

In the above equation we have defined $\Omega = \omega l/c$, $\beta = \hat{\beta} l$, and hence all quantities appearing are dimensionless. We have used two-scale expansions of the fractions r_0/r and r_0^2/r^2 such that their short-scale dependence is retained consistently; these are given in appendix A.

Having made the expansion (2.5), we collect terms of matching orders in η, resulting in a hierarchy that is to be solved upwards from the lowest order. Crucially, the leading order equation is simply that of a layered stack, which permits Bloch wave solutions and so we can proceed along the lines of HFH, seeking solutions in the form of an ansatz:

$$H(R,\xi) = \sum_{j=0}^{\infty} \eta^j H_j(R,\xi), \qquad E(R,\xi) = \sum_{j=0}^{\infty} \eta^j E_j(R,\xi), \qquad \Omega^2 = \sum_{j=0}^{\infty} \eta^j \Omega_j^2. \tag{2.6}$$

At leading order, this yields an eigenvalue problem for the one-dimensional Helmholtz system:

$$\left\{ \frac{\partial^2}{\partial \xi^2} + k_i^2 \right\} \begin{pmatrix} H_0(R,\xi) \\ E_0(R,\xi) \end{pmatrix} = 0, \tag{2.7}$$

where $k_i = (n_i^2\Omega_0^2 - \beta^2)^{1/2}$ for $i = 1,2$ is the dimensionless transverse wavenumber in each layer at the standing wave frequency, which will appear frequently in what follows. We supply anti-periodic or periodic boundary conditions on the short-scale, and the resulting asymptotic solutions are thus valid for frequencies inside the band gap and in the vicinity of a standing wave eigenfrequency Ω_0. Equation (2.7) is independent of the long-scale R coordinate and only depends upon the short-scale ξ coordinate, so we solve it on an arbitrary single cell. Continuity conditions at the interface joining the two materials are derived from the leading order terms in the two-scale expansions of (2.3) and (2.4), and are given by

$$[E_0] = 0, \qquad \left[-\frac{i\mu_i\Omega_0}{k_i^2}H_{0,\xi}\right] = 0 \qquad [H_0] = 0, \qquad \left[\frac{i\varepsilon_i\Omega_0}{k_i^2}E_{0,\xi}\right] = 0. \tag{2.8}$$

We observe that, to leading order, the continuity conditions decouple, meaning that in most cases the modes will predominantly either be TE, with the coupled TM components not appearing at leading order, or vice versa. We thus deduce that weak coupling, at most, will be induced by the curvature, noting that in the case of an infinite layered stack there is none at all. For the stack, the first band gap satisfying the condition $\Omega > \beta$ (necessary for propagating solutions in the hollow-core case) lies between two anti-periodic eigenmodes, as shown in Fig. 2.

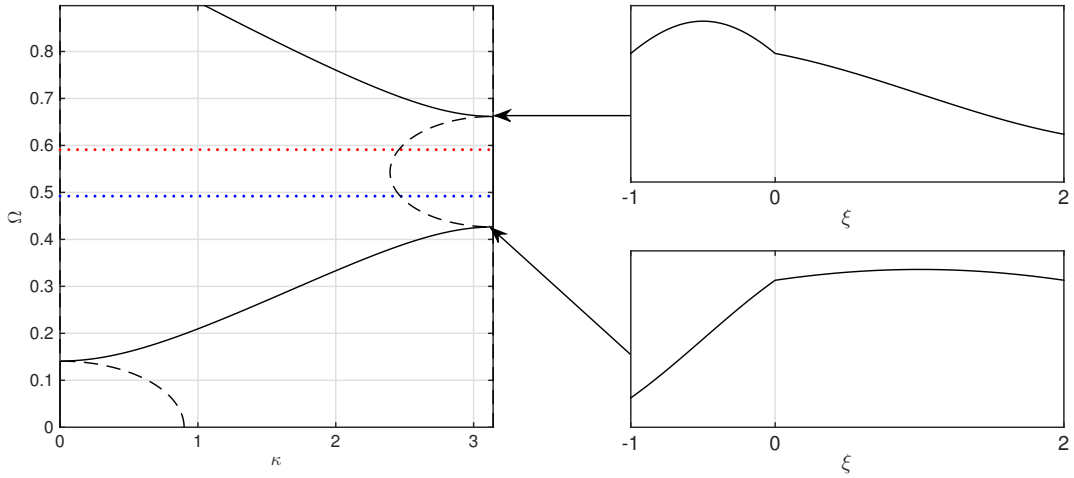


FIG. 2: Photonic band diagram for a layered dielectric stack ($n_1 = 3$, $n_2 = 1.5$, $\alpha = 2$), at oblique incidence ($\beta = 0.3$) in the TE case, including the imaginary part of the wavenumber (dashed) in the photonic band gaps. The right hand panels show the longitudinal magnetic field $h_0(\xi)$ for the lowest two anti-periodic eigenmodes. The blue (red) dotted line is the frequency of the lowest $m = 0$ ($m = 1$) mode for a hollow-core Bragg fiber with a core radius $r_0 = 10l$.

Assuming an open band gap exists in the vicinity of the eigenvalue in question (which will not be true in the case of a repeated eigenvalue), the standing wave solution to (2.7) is unique up to a multiplicative coefficient, which is generally a function of the long-scale coordinate R. The solution is thus given by $H_0 = f_0(R)h_0(\xi)$, $E_0 = 0$ in the TE-dominated case for an arbitrary function f_0, and $E_0 = f_0(R)e_0(\xi)$, $H_0 = 0$ in the TM-dominated case. In the TE-dominated case, the eigenfrequency Ω_0 is a solution of the equation

$$2k_1k_2\mu_1\mu_2(1+\cos k_1\cos k_2\alpha) - (k_1^2\mu_2^2 + k_2^2\mu_1^2)\sin k_1\sin k_2\alpha = 0, \tag{2.9}$$

and explicit solutions for the eigenmodes are given in appendix D. To obtain the TM-dominated modes, we simply make the substitutions $\mu_i \leftrightarrow \varepsilon_i$ in these expressions.

Having solved the standing wave eigenvalue problem at leading order, we continue up the asymptotic hierarchy to the $O(\eta)$ system, which yields an inhomogeneous problem for the same one-dimensional Helmholtz operator as before:

$$\left\{\frac{\partial^2}{\partial\xi^2}+k_i^2\right\}\begin{pmatrix} H_1 \\ E_1 \end{pmatrix} = \left\{-2\frac{\partial^2}{\partial R\partial\xi}-\frac{1}{R}\frac{\partial}{\partial\xi}-n_i^2\Omega_1^2\right\}\begin{pmatrix} H_0 \\ E_0 \end{pmatrix}. \tag{2.10}$$

Periodic/anti-periodic boundary conditions are applied as before, and continuity conditions given by

$$[E_1]=0, \quad \left[\frac{\beta m E_0}{k_i^2}\frac{1}{R}-\frac{i\mu_i\Omega_0}{k_i^2}\left(H_{1,\xi}+H_{0,R}\right)+\frac{i\mu_i\Omega_1^2 H_{0,\xi}}{k_i^2}\left(\frac{\Omega_0}{k_i^2}-\frac{1}{2\Omega_0}\right)\right]=0, \tag{2.11}$$

$$[H_1]=0, \quad \left[\frac{\beta m H_0}{k_i^2}\frac{1}{R}+\frac{i\varepsilon_i\Omega_0}{k_i^2}\left(E_{1,\xi}+E_{0,R}\right)-\frac{i\varepsilon_i\Omega_1^2 E_{0,\xi}}{k_i^2}\left(\frac{\Omega_0}{k_i^2}-\frac{1}{2\Omega_0}\right)\right]=0. \tag{2.12}$$

In appendix B we derive a compatibility condition that implies $\Omega_1 = 0$, which simplifies the above conditions significantly. As was the case at leading order, the resulting solution is separated due to the independence of the disparate coordinate variables. In the TE-dominated case, we have $H_1 = f_0(R)\hat{h}_1(\xi)/R + f_{0,R}(R)h_1(\xi) + f_1(R)h_0(\xi)$, where f_1 is another arbitrary function, and the electric field at this order is generally non-zero, and given by $E_1 = f_0(R)\hat{e}_1(\xi)/R$. Explicit solutions are given in appendix D and TM-dominated modes are treated analogously.

Having solved the $O(\eta)$ system, we move onto the next and final order necessary for our analysis, which yields a second inhomogeneous problem:

$$\begin{aligned}\left\{\frac{\partial^2}{\partial\xi^2}+k_i^2\right\}\begin{pmatrix} H_2 \\ E_2 \end{pmatrix} &= \left\{-2\frac{\partial^2}{\partial R\partial\xi}-\frac{1}{R}\frac{\partial}{\partial\xi}\right\}\begin{pmatrix} H_1 \\ E_1 \end{pmatrix} \\ &+\left\{-\frac{\partial^2}{\partial R^2}-\frac{1}{R}\frac{\partial}{\partial R}+\frac{\xi}{R^2}\frac{\partial}{\partial\xi}+\frac{m^2}{R^2}-n_i^2\Omega_2^2\right\}\begin{pmatrix} H_0 \\ E_0 \end{pmatrix},\end{aligned} \tag{2.13}$$

with boundary conditions

$$[E_2]=0, \quad \left[\frac{\beta m E_1}{k_i^2}\frac{1}{R}-\frac{\beta m\xi E_0}{k_i^2}\frac{1}{R^2}-\frac{i\mu_i\Omega_0}{k_i^2}\left(H_{2,\xi}+H_{1,R}\right)+\frac{i\mu_i\Omega_2^2 H_{0,\xi}}{k_i^2}\left(\frac{\Omega_0}{k_i^2}-\frac{1}{2\Omega_0}\right)\right]=0, \tag{2.14}$$

$$[H_2]=0, \quad \left[\frac{\beta m H_1}{k_i^2}\frac{1}{R}-\frac{\beta m\xi H_0}{k_i^2}\frac{1}{R^2}+\frac{i\varepsilon_i\Omega_0}{k_i^2}\left(E_{2,\xi}+E_{1,R}\right)-\frac{i\varepsilon_i\Omega_2^2 E_{0,\xi}}{k_i^2}\left(\frac{\Omega_0}{k_i^2}-\frac{1}{2\Omega_0}\right)\right]=0. \tag{2.15}$$

Thankfully, we are spared from solving this system, and only need to derive a compatibility condition analogous to that found at the previous order (see appendix C). The result of this is an ODE satisfied by the long-scale function $f_0(R)$:

$$\frac{\mathrm{d}^2 f_0}{\mathrm{d}R^2}+\frac{c_1}{R}\frac{\mathrm{d}f_0}{\mathrm{d}R}+\left(\Omega_2^2c_2^2-\frac{c_3^2}{R^2}\right)f_0=0. \tag{2.16}$$

The coefficients c_i are made up of integrals of the leading and first order solutions that have been found explicitly. Equation (2.16) is the main result of this article; the concentric cylindrical layered structure is

effectively replaced by this single ordinary differential equation, posed entirely on the radial long-scale. The short-scale, potentially highly-oscillatory behaviour, is encapsulated within the coefficients c_1, c_2 and c_3. We recall that in the TE case, the full field is given to leading order by $H_0 = f_0(R)h_0(\xi)$; a periodic short-scale Bloch solution $h_0(\xi)$ is modulated by a long-scale envelope function $f_0(R)$.

2.3 *Effective eigenvalue problem*

Having treated the cladding region asymptotically, we have the necessary elements to solve an effective eigenvalue problem for guided modes in the fiber. Strictly speaking, equation (2.16) applies in the bulk region of the cladding, and gives the asymptotic form of the solution as $r \to \infty$ away from the boundary at $r = r_0$. In order to reflect this, one approach would be to treat N inner layer pairs exactly using, for example, the matrix method of Yeh et al. (1978), and then to connect this with the asymptotic solution starting at $r = r_0 + Nl(1+\alpha)$. Clearly, the larger the value of N, the more accurate the solution, and its associated eigenvalue, will be. A similar approach was employed in Xu et al. (2002) and, as was the case there, this also allows us to treat small-core fibers. In fact, as we shall demonstrate, even the crudest approximation with $N = 0$ yields results with surprising accuracy.

In the core region, the solution for the z-component of each field in equation (2.2) is given by a Bessel function of the first kind:

$$\begin{pmatrix} H(r) \\ E(r) \end{pmatrix} = \begin{pmatrix} \gamma_1 \\ \gamma_2 \end{pmatrix} J_m(\kappa_0 r/l), \tag{2.17}$$

where $\kappa_0 = (n_0^2\Omega^2 - \beta^2)^{1/2}$ and γ_1, γ_2 are arbitrary constants.

In the cladding region, we need to solve the effective equation (2.16). After multiplying by R^2, we identify this as a transformed Bessel equation as considered in, say, Bowman (1958), and the solution of this, decaying at infinity, is given by

$$f_0(R) = R^{(1-c_1)/2} K_q\left(|\Omega_2 c_2| R\right), \tag{2.18}$$

where $q = \sqrt{(c_1-1)^2/4 + c_3^2}$, and without loss of generality we have set the arbitrary constant coefficient of the solution to unity. We note that the order q of the modified Bessel function may be real or imaginary, a subject dealt with in detail in Dunster (1989).

The core solution (2.17) must be connected to the cladding solution (2.18) using effective boundary conditions, which are derived from the electromagnetic boundary conditions (2.3) and (2.4). In order to do so, we consider the full asymptotic solution in the cladding region, which is given in the TE case by

$$H(R,\xi) = f_0(R)h_0(\xi) + \eta\left(f_0(R)\hat{h}_1(\xi)/R + f_{0,R}(R)h_1(\xi) + f_1(R)h_0(\xi)\right) + O(\eta^2), \tag{2.19}$$

$$E(R,\xi) = \eta f_0(R)\hat{e}_1(\xi)/R + O(\eta^2). \tag{2.20}$$

Substituting back to the original radial coordinate variable r, these expressions are matched with those in (2.17) at $r = r_0$ using the continuity conditions (2.4), neglecting higher-order terms. For a purely TE mode ($m = 0$ and/or $\beta = 0$), the longitudinal electric field is zero in both regions, and without loss of generality we may set $f_1 = 0$ (equivalent to redefining $f_0 \to f_0 + \eta f_1$). In this case, the two conditions in (2.4) are sufficient to fix the two unknowns γ_1 and Ω_2. In the case that $m \neq 0$ and $\beta \neq 0$, we additionally use the first and second condition in (2.3) to eliminate γ_2 and f_1 respectively. The aim is to find values

of Ω_2 that solve the resulting equations. When these are substituted into the ansatz (2.6), they give the frequencies of the guided modes.

At this point we stress that each band gap is bounded from above and from below by standing wave eigenfrequencies. In applying the asymptotic method, we regard one of these as Ω_0, and expect to find guided modes of the fiber whose frequencies are in its vicinity. The solutions will be accurate provided that $\Omega_2^2 = O(1)$.

3. Results

As an initial application of the method described herein, we calculate the dispersion of the fundamental $m = 0$ guided mode in a hollow-core fiber with the following material parameters: $n_1 = 3$, $n_2 = 1.5$, and $r_0 = 10l$, which are the same as those used in Xu et al. (2000). The ratio between layer thicknesses is chosen for optimal confinement (i.e. the reciprocal of the ratio of refractive indices, $\alpha = 2$). We treat the problem first using the asymptotic theory alone, connecting the homogenised cladding directly to the core solution at $r = r_0$, and then also by treating one layer pair exactly, then connecting this solution to the asymptotic one at $r = r_0 + l(1+\alpha)$. The results are shown in Table 1, and plotted in Figure 3. In Figure 4 we show a TE-dominated propagating $m = 1$ mode in the same fiber. In both cases, we also treat the problem using a 2D FEM simulation with the Comsol Wave Optics® module, where a large number of layers is considered and perfect electrical conducting conditions applied at the outer boundary.

Table 1: Dispersion of the fundamental TE mode (m = 0) for a hollow-core fibre with parameter values $n_1 = 3$, $n_2 = 1.5$, $r_0 = 10l$, $\alpha = 2$. Separate columns are included for solutions calculated asymptotically with no exactly-treated layers ($N = 0$) and for solutions where one layer pair is treated exactly ($N = 1$). We also include separate columns for frequencies calculated as upward (↑) and downward (↓) perturbations from the two bounding standing wave frequencies. FEM-calculated frequencies are included for comparison.

β	Ω_{FEM}	$\Omega_{N=0}\uparrow$	$\Omega_{N=1}\uparrow$	$\Omega_{N=0}\downarrow$	$\Omega_{N=1}\downarrow$
0	0.415	0.416	0.415		
0.05	0.418	0.422	0.417		
0.10	0.423	0.426	0.422		
0.15	0.433	0.436	0.432		
0.20	0.448	0.449	0.448		
0.25	0.469	0.476	0.468		
0.30	0.493	0.493	0.492		
0.35	0.522	0.525	0.523	0.516	0.521
0.40	0.554	0.546	0.553	0.548	0.554
0.45	0.589			0.593	0.591
0.50	0.626			0.624	0.626
0.55	0.664			0.662	0.663
0.60	0.703			0.700	0.700
0.65	0.743			0.741	0.743

The asymptotic theory evidently works well with the parameters chosen above. In the $N = 0$ case, the relative error appears to be random, and does not exceed 2%. This suggests that the source of inaccuracy is mainly due to the bolting of the core solution to the cladding, rather than the approximation of the cladding itself, which we would expect to give rise to a systematic error. This is perhaps unsurprising,

as the cladding solution was derived under the assumption of the layered structure being infinite, and we expect that in the vicinity of $r = r_0$ the solution will be altered. Further evidence for this is found by considering the $N = 1$ case in which one layer pair is treated exactly, in which case the random error is reduced to less than 0.4% throughout the range considered, suggesting that the majority of the error is due to the disparity between the asymptotic and exact solutions in the first pair of layers. In Figure 5 we plot the relative error against β for both cases.

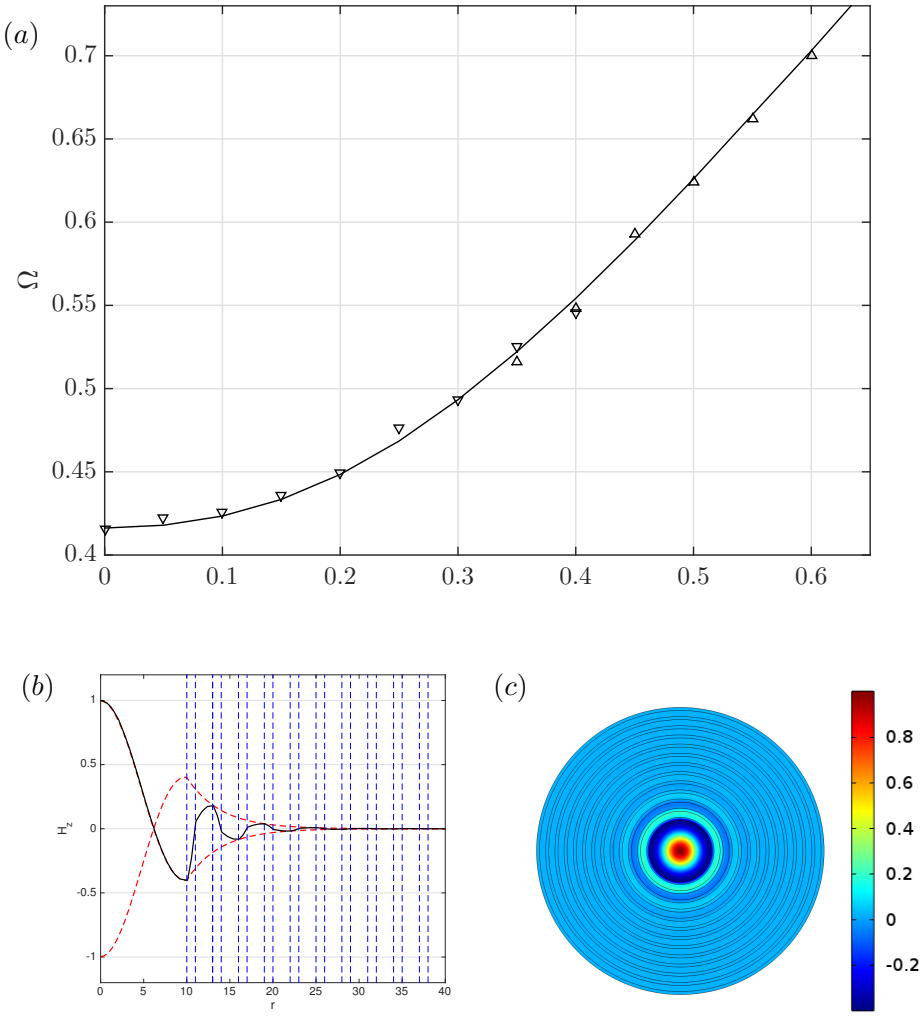


FIG. 3: (a) Dispersion of the fundamental TE mode for the fiber described in Table 1. Symbols correspond to frequencies calculated using the asymptotic method with no layers treated exactly ($N = 0$), and lines correspond to those calculated using FEM simulation. The relative error between the two does not exceed 2%. (b) shows the longitudinal magnetic field for $\beta = 0.3$, calculated using FEM, with the dashed red lines showing the envelope function f_0 calculated using the asymptotic method. The agreement is clearly excellent. (c) shows a colour plot of the magnetic field for the same mode.

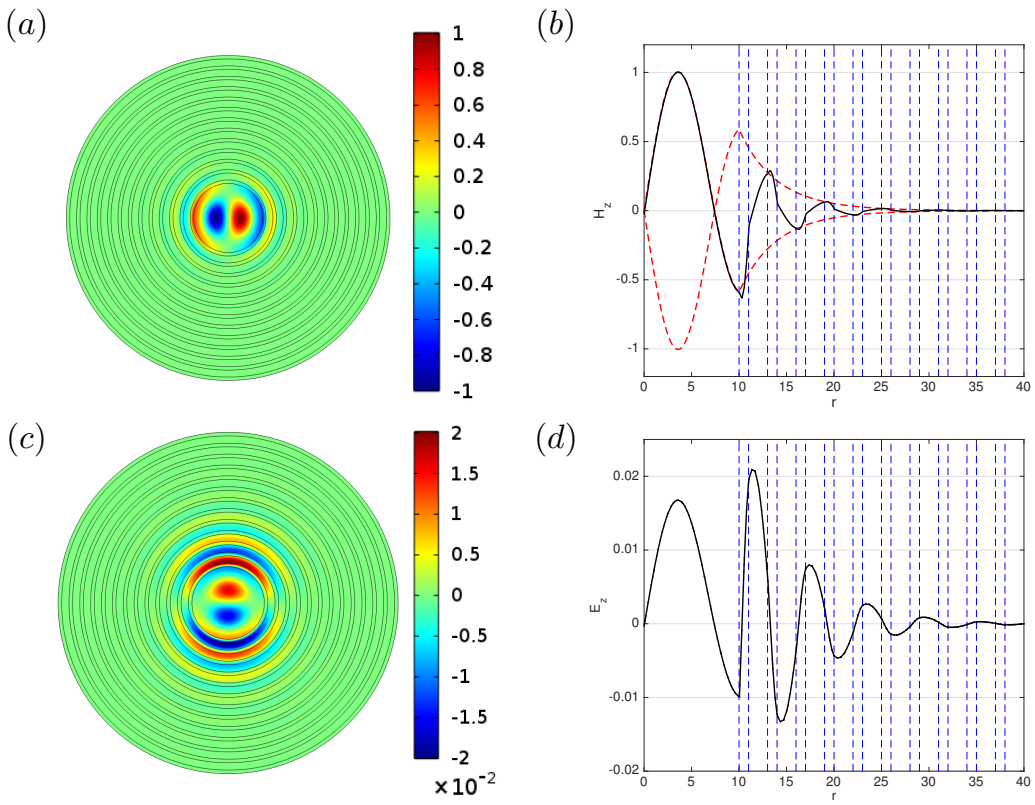


FIG. 4: Mixed TE-dominated mode with azimuthal number $m = 1$ for a fiber with $n_1 = 3$, $n_2 = 1.5$, $r_0 = 10l$, $\alpha = 2$, with proapagation constant $\beta = 0.3$. (a) and (b) show the longitudinal magnetic field H_z, calculated using the finite element method, with the red dashed line in (b) showing the envelope function calculated using the asymptotic approximation (with no layers treated exactly). (c) and (d) show the longitudinal electric field E_z. Note the disparity in magnitude between the two fields, which is made apparent in the non-dimensional setting. The frequency calculated with the asymptotic method is $\Omega = 0.594$, which represents a 1.3% error compared with the FEM-calculated value of 0.602.

In order to assess the utility of the asymptotic method, it is useful to consider parameter regimes in which the theory is likely to break down. One obvious such limit is when the core radius becomes comparable in size to the layer thickness, in which case $\eta \ll 1$ no longer holds and we do not expect a separation of scales to occur in the first few layers of the cladding. To investigate this, we consider the evolution of the modes of two different fibers as the core radius is decreased. In each case, we fix the physical parameters of the fiber and the propagation constant β, and calculate the frequency of the modes for different values of η, which are then compared with full FEM simulation. In Figure 6 we consider the non-propagating $\beta = 0$ modes with $m = 0, 1$ for a fiber with relatively low refractive index layers, and in Figure 7 we consider propagating modes with $\beta = 0.3$, $m = 0, 1$ for a fiber with higher

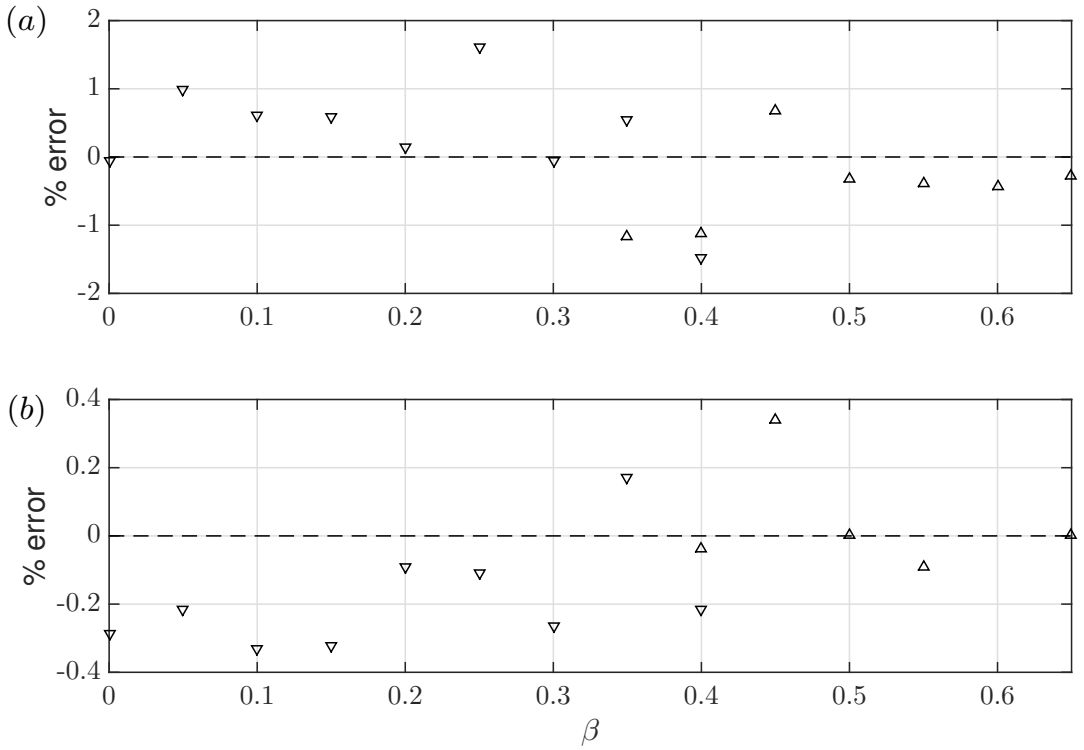


FIG. 5: Relative error in Ω for the example considered in Table 1 and Figure 3, plotted as a function of the dimensionless propagation constant β. Frames (a), (b) correspond to the cases $N = 0$, $N = 1$ respectively.

index layers. In both cases, we observe that the relative error for the asymptotic theory with $N = 0$ is random and less than 2%, as we observed in the previous example, but for $\eta \approx 0.15$ and greater the error starts to build systematically, with the asymptotic theory tending to overestimate the frequency of the modes. As mentioned before, in the case of small-core fibers, the asymptotic theory can still be used, but for accurate results a number of exactly-treated layers should be included between the core and the homogenised cladding layer such that $\eta = l/r_0$ can be considered small, where r_0 now denotes the radius at which the asymptotic scheme is applied from.

A second regime under which we might expect the asymptotic scheme to fail is when the contrast between layers becomes too great. High contrasts are associated with large band gaps and these can lead to very high degrees of confinement, under which conditions it is likely that a separation of scales will not occur. To investigate this, we consider the fundamental non-propagating $\beta = 0$ mode for a hollow-core fiber with equal layer thicknesses ($\alpha = 1$) and a core radius of $r_0 = 10l$, which we have seen is sufficiently large for the asymptotic scheme to work in principle. We fix the refractive index of the second layer $n_2 = 1$, and increase n_1. The scheme appears to work reasonably well until $n_1 \approx 4$, beyond which a systematic error begins to accumulate, with the scheme tending to overestimate the frequency.

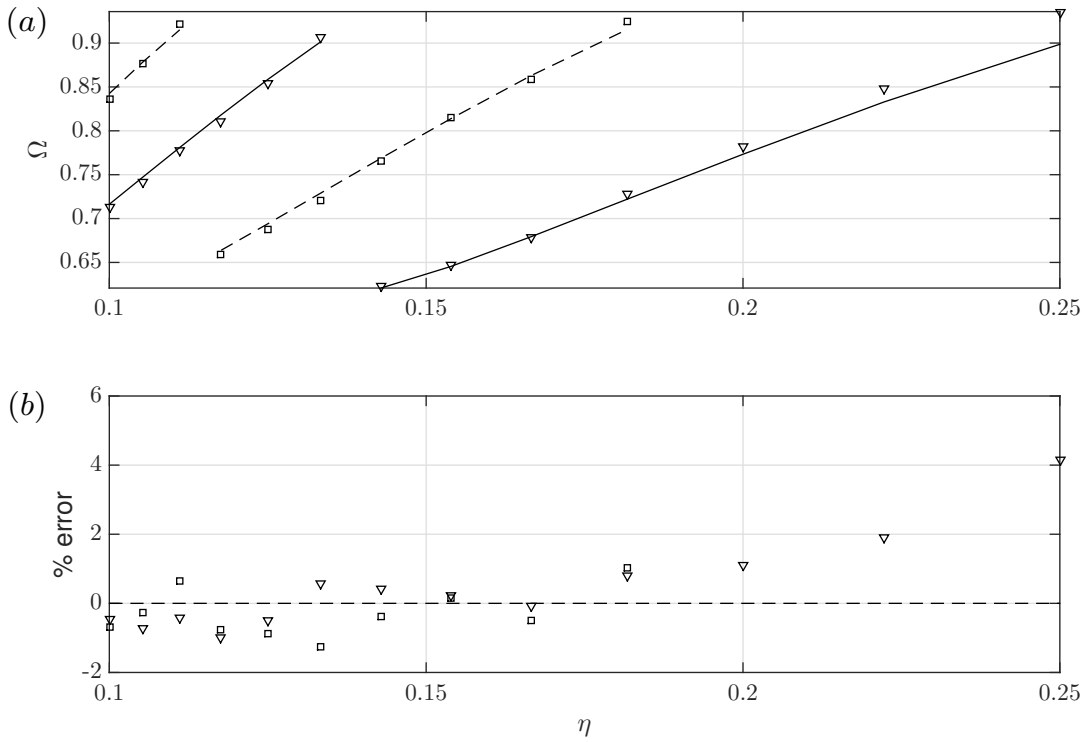


FIG. 6: (a) Evolution of the non-propagating $\beta = 0$ modes for a hollow-core fiber with $n_1 = 2$, $n_2 = 1$, $\alpha = 2$ as the core radius decreases and hence η increases. The solid (dashed) line are the frequencies of the $m = 0$ ($m = 1$) modes calculated using full FEM simulation, and the triangles (squares) are the corresponding values calculated using the asymptotic method with $N = 0$. (b) shows the relative error between the two, using the same symbols.

Although the error remains considerably smaller in the $N = 1$ case, the same trend is observed in both the $N = 0$ and $N = 1$ cases, suggesting that the systematic error is a result of the asymptotic scheme breaking down in the bulk of the cladding, rather than being caused by the bolting of solutions at $r = r_0$.

4. Concluding remarks

We have demonstrated that a two-scale asymptotic method based on high-frequency homogenisation can be used to calculate the frequencies and field patterns for guided modes in a cylindrical Bragg fiber. A physical picture emerges where the solution in the bulk of the cladding is a modulated (anti-)periodic function of the radial distance, where the modulation is governed by a long-scale Bessel-like equation given by (2.16). In order to connect this to the simple core solution, an asymptotic 'boundary layer' region should be considered whose asymptotic limit as $r \to \infty$ is given by the result of the asymptotic scheme. This is a challenging problem that is beyond the scope of this paper, but an interesting possibility for further work. Instead, we use a cruder 'bolting together' of solutions in the two separate regions; the effective equation governing the field in the layered cladding region is directly connected to the core solution using continuity conditions. In order to assess the error introduced by doing this,

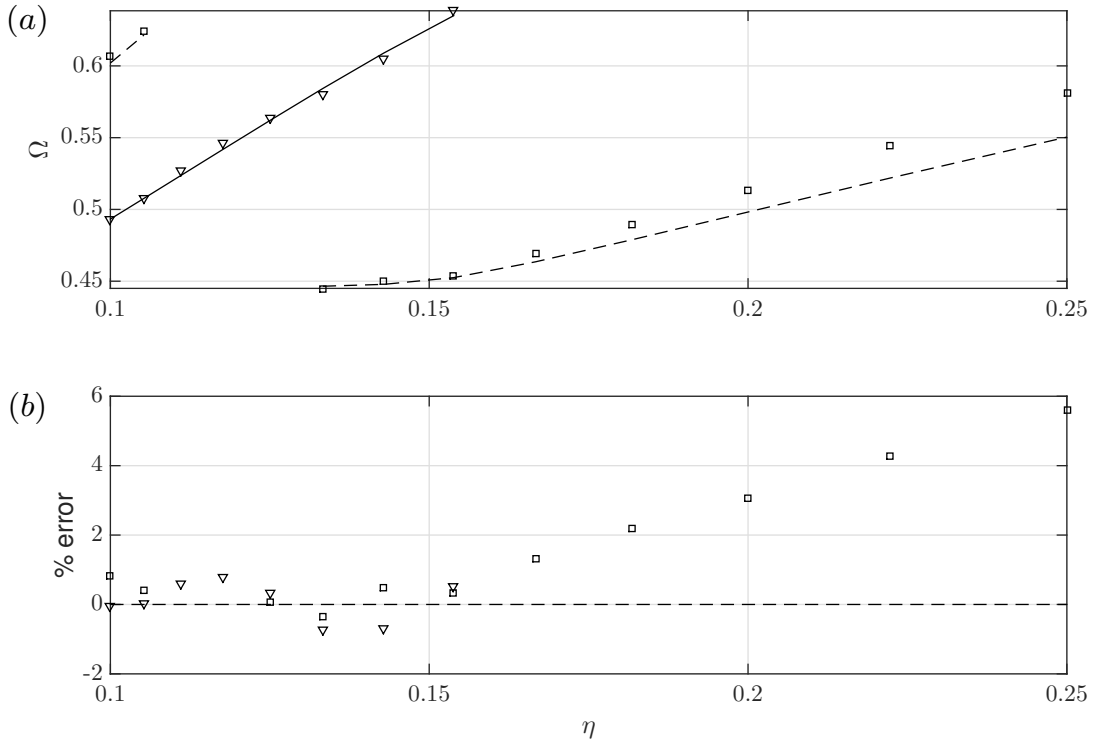


FIG. 7: (a) Evolution of the propagating $\beta = 0.3$ modes for a hollow-core fiber with $n_1 = 3$, $n_2 = 1.5$, $\alpha = 2$ as the core radius decreases and hence η increases. The solid (dashed) line are the frequencies of the $m = 0$ ($m = 1$) modes calculated using full FEM simulation, and the triangles (squares) are the corresponding values calculated using the asymptotic method with $N = 0$. (b) shows the relative error between the two, using the same symbols.

we have considered connecting the two regions via a single pair of exactly-treated inner layers, which in the cases considered significantly reduces the disparity between the asymptotic results and the full FEM results. This suggests that the boundary effects at $r = r_0$ are responsible for the majority of the error in the scheme. We note that increasing N, the number of exactly-treated pairs, would also allow small-core fibers to be treated, for which the method would otherwise fail. In the parameter regime where the asymptotic scheme can be applied, the accuracy of the calculated eigenvalues is similar to that reported in Xu et al. (2000, 2002), in which a different asymptotic method was used. However, if the contrast between layers is increased too much, the scheme fails to give accurate approximations as the separation of scales assumption breaks down.

Treating the work herein as a canonical example, we have demonstrated in principle that high-frequency homogenisation methods may be used to study the guided modes of a microstructured optical fiber. A natural extension of this work would be to extend this to other types of fiber, such as PCFs. In that case, further difficulties will be introduced due to the two-dimensional Brillouin zone, as well as the need to treat the boundary layer surrounding the fiber's core with a greater degree of sophistication.

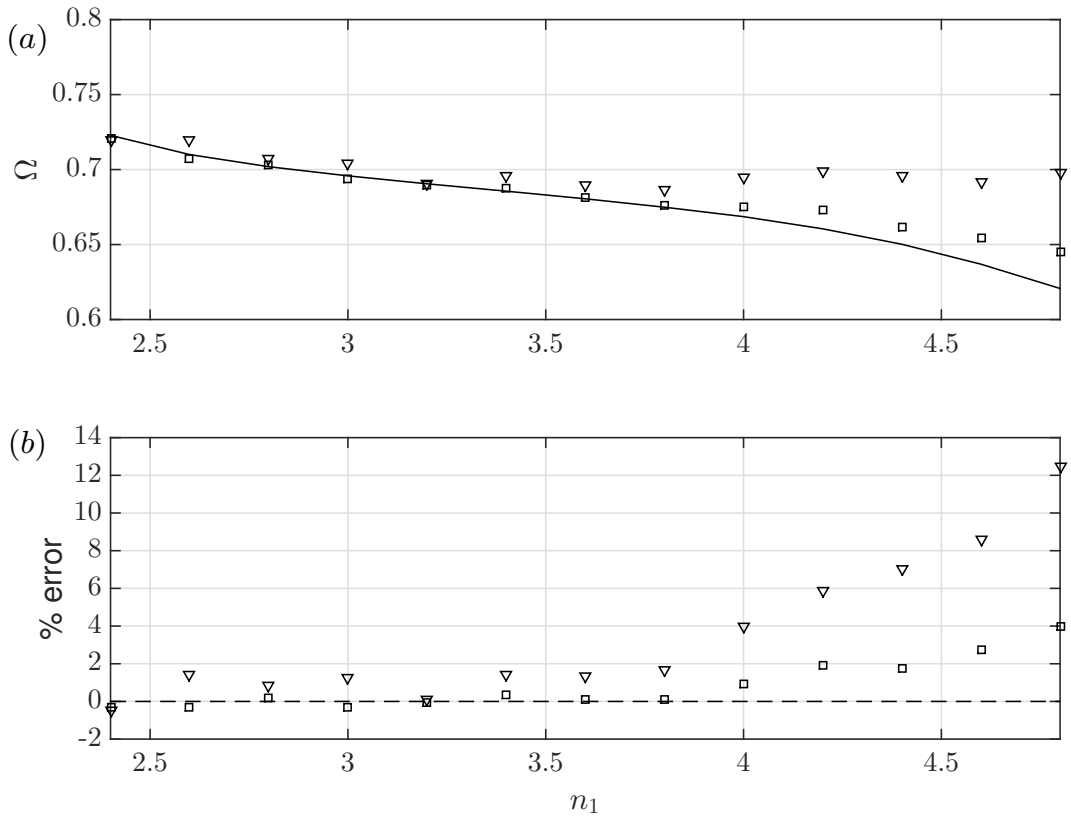


FIG. 8: (a) Evolution of the non-propagating $\beta = 0$, $m = 0$ mode for a hollow-core fiber with $n_2 = 1$, $\alpha = 1$, $r_0 = 10l$ as the refractive index n_1 is increased. The solid line shows the frequency calculated using full FEM simulation, and the triangles (squares) are the corresponding values calculated using the asymptotic method with $N = 0$ ($N = 1$). (b) shows the relative error between the asymptotic and FEM results, using the same symbols.

Acknowledgment

RVC thanks the EPSRC (UK) for their support through research grants EP/L024926/1 & EP/J009636/1.

REFERENCES

Bakhvalov, N. & Panasenko, G. (1989) *Homogenisation: averaging processes in periodic media*. Springer-Verlag, Düsseldorf.

Bensoussan, A., Lions, J. & Papanicolaou, G. (1978) *Asymptotic analysis for periodic structures*. North-Holland, Amsterdam.

Bowman, F. (1958) *Introduction to Bessel Functions*. Dover, New York.

Chigrin, D. N., Lavrinenko, A. V., Yarotsky, D. A. & Gaponenko, S. V. (1999) Observation of Total Omnidirectional Reflection from a One-Dimensional Dielectric Lattice. *Appl. Phys. A*, **68**, 25.

Craster, R. V., Kaplunov, J. & Pichugin, A. V. (2010) High-frequency homogenization for periodic media.. *Proc. R. Soc. Lond*, **466**, 2341–2362.

Dunster, T. (1989) Bessel Functions of Purely Imaginary Order, with an Application to Second-Order Linear Dif-

ferential Equations Having a Large Parameter. *SIAM J. Math. Anal.*, **21**(4), 995–1018.

Fink, Y., Ripin, D. J., Fan, S., Chen, C., Joannopoulos, J. D. & Thomas, E. L. (1999) Guiding Optical Light in Air Using an All-Dielectric Structure. *J. Lightwave Technol.*, **17**(11), 2039–2041.

Fink, Y., Winn, J. N., Fan, S., Chen, C., Michel, J., Joannopoulos, J. D. & Thomas, E. L. (1998) A Dielectric Omnidirectional Reflector. *Science*, **282**, 1679–1682.

Guenneau, S., Poulton, C. & Movchan, A. (2003) Oblique propagation of electromagnetic and elastic waves for an array of cylindrical fibres. *Proc. R. Soc. Lond. A*, **459**, 2215–2263.

Joannopoulos, J., Johnson, S., Winn, J. & Meade, R. (2011) *Photonic Crystals: Molding the Flow of Light (Second Edition)*. Princeton University Press.

Joannopoulos, J. D., Johnson, S. G., Winn, J. N. & Meade, R. D. (2008) *Photonic Crystals, Molding the Flow of Light*. Princeton University Press, Princeton, second edition.

Markos, P. & Soukoulis, C. M. (2008) *Wave Propagation: From Electrons to Photonic Crystals and Left-Handed Materials*. Princeton University Press.

Mizrahi, A. & Schächter, L. (2004) Bragg reflection waveguides with a matching layer. *Opt. Express*, **12**(4), 3156–3170.

Oleinik, O., Shamaev, A. & Yosifian, G. (1992) *Mathematical problems in elasticity and homogenization*. North-Holland, Amsterdam.

Russell, P. S. J. (2003) Photonic crystal fibers. *Science*, **299**, 358362.

Temelkuran, B., Hart, S. D., Benoit, G., Joannopoulos, J. D. & Fink, Y. (2002) Wavelength-scalable hollow optical fibres with large photonic bandgaps for CO_2 laser transmission. *Nature*, **420**, 650–653.

Volodin, B. L., Dolgy, S. V., Melnik, E. D., Downs, E., Shaw, J. & Ban, V. S. (2004) Wavelength stabilization and spectrum narrowing of high-power multimode laser diodes and arrays by use of volume Bragg gratings. *Optics Letters*, **29**, 1891–1893.

Wu, F., Guo, S., Ikram, K., Albin, S., Tai, H. & Rogowski, R. S. (2005) Numerical analysis of Bragg fibers using a compact 1D finite-difference frequency-domain method. *Opt. Comm.*, **21**(1), 165–174.

Xu, Y., Lee, R. K. & Yariv, A. (2000) Asymptotic analysis of Bragg fibers. *Opt. Lett.*, **25**(24), 1756–1758.

Xu, Y., Ouyang, G. K. & Lee, R. K. (2002) Asymptotic Matrix Theory of Bragg Fibers. *J. Lightwave Technol.*, **20**(3), 428–440.

Yeh, P., Yariv, A. & Hong, C. (1977) Electromagnetic propagation in periodic stratified media. I. General theory.. *JOSA*, **67**, 423–438.

Yeh, P., Yariv, A. & Marom, E. (1978) Theory of Bragg fiber. *JOSA*, **68**(9), 1196–1201.

Zhikov, V., Koslov, S. & Oleinik, O. (1994) *Homogenization of differential operators and integral functionals*. Springer-Verlag, Düsseldorf.

Zolla, F., Renversez, G., Nicolet, A., Kuhlmey, B., Guenneau, S. & Felbacq, D. (2005) *Foundations of photonic crystal fibres*. Imperial College Press, London.

A. Two-scale representation of r_0/r and r_0^2/r^2

We consider the j^{th} cell from the inner boundary of the layered cladding region, and hence write $r = r_0 + \{(1+\alpha)j - \alpha + \xi\}l$. Expanding r_0/r using the binomial theorem:

$$\frac{r_0}{r} = \frac{r_0}{r_0 + \{(1+\alpha)j-\alpha\}l}\left[1 - \frac{\xi l}{r_0 + \{(1+\alpha)j-\alpha\}l} + O\left(\frac{l}{r_0 + \{(1+\alpha)j-\alpha\}l}\right)^2\right].$$

Remembering that $\eta = l/r_0$ leaves us with

$$\frac{r_0}{r} = \frac{r_0}{r_0 + \{(1+\alpha)j-\alpha\}l} - \eta\xi\left(\frac{r_0}{r_0 + \{(1+\alpha)j-\alpha\}l}\right)^2 + O(\eta^2), \tag{A.1}$$

which yields immediately

$$\frac{r_0^2}{r^2} = \left(\frac{r_0}{r_0 + \{(1+\alpha)j - \alpha\}l}\right)^2 - 2\eta\xi\left(\frac{r_0}{r_0 + \{(1+\alpha)j - \alpha\}l}\right)^3 + O(\eta^2). \tag{A.2}$$

The correct two-scale expansions for the above fractions are thus

$$\frac{r_0}{r} = \frac{1}{R} - \eta\xi\left(\frac{1}{R}\right)^2 + O(\eta^2), \tag{A.3}$$

$$\frac{r_0^2}{r^2} = \left(\frac{1}{R}\right)^2 - 2\eta\xi\left(\frac{1}{R}\right)^3 + O(\eta^2). \tag{A.4}$$

B. $O(\eta)$ compatibility condition

In this section we derive the result $\Omega_1 = 0$ as a compatibility condition for the system (2.10). For convenience, for any function of the short-scale variable ξ, let us introduce the notation $[f(\xi)]_{c,d}^{a,b} = f(a) + f(b) - f(c) - f(d)$. We begin by dividing the first lines of (2.7) and (2.10) by k_i^2, yielding in each layer:

$$\frac{1}{k_i^2}h_{0,\xi\xi} + h_0 = 0, \tag{B.1}$$

$$\frac{1}{k_i^2}H_{1,\xi\xi} + H_1 = -\frac{1}{k_i^2}\left(2H_{0,R\xi} + \frac{1}{R}H_{0,\xi} + n_i^2\Omega_1^2 H_0\right). \tag{B.2}$$

Subtracting the product of (B.2) with h_0 from the product of (B.1) with H_1 and integrating over the cell yields

$$\left[\frac{1}{k_i^2}\left(h_{0,\xi}H_1 - H_{1,\xi}h_0\right)\right]_{0^+,-1}^{0^-,\,\alpha} = \int_{-1}^{\alpha}\frac{1}{k_i^2}\left(2H_{0,R\xi}h_0 + \frac{1}{R}H_{0,\xi}h_0 + n_i^2\Omega_1^2 H_0 h_0\right)\mathrm{d}\xi. \tag{B.3}$$

Using the continuity conditions (2.8), along with (anti-)periodicity, we find that the first term on the left vanishes. Integrating the first two terms on the right then leaves

$$\left[\frac{1}{k_i^2}\left((H_{1,\xi} + H_{0,R})h_0 + \frac{1}{2R}H_0 h_0\right)\right]_{0^+,-1}^{0^-,\,\alpha} = -\Omega_1^2\int_{-1}^{\alpha}\frac{1}{k_i^2}n_i^2 H_0 h_0 \mathrm{d}\xi. \tag{B.4}$$

Using the continuity conditions (2.11), remembering that $E_0 \equiv 0$, we have

$$\left[\frac{1}{k_i^2}\frac{1}{2R}H_0 h_0\right]_{0^+,-1}^{0^-,\,\alpha} = -\Omega_1^2\left\{\int_{-1}^{\alpha}\frac{1}{k_i^2}n_i^2 H_0 h_0 \mathrm{d}\xi + \left[\frac{1}{k_i^2}\left(\frac{1}{k_i^2} - \frac{1}{2\Omega_0^2}\right)H_{0,\xi}h_0\right]_{0^+,-1}^{0^-,\,\alpha}\right\}. \tag{B.5}$$

From the symmetry of the leading order solution $h_0(\xi)$, the term on the left vanishes. Using the boundary conditions (2.8) along with the ODE (2.7), the remaining equation becomes

$$0 = \Omega_1^2 f_0\int_{-1}^{\alpha}\frac{1}{k_i^2}\left((n_i^2 - 1)|h_0|^2 + \frac{1}{k_i^2}|h_{0,\xi}|^2\right)\mathrm{d}\xi. \tag{B.6}$$

Assuming that $n_i > 1$, the only possibility for non-trivial solutions is that $\Omega_1 = 0$.

C. $O(\eta^2)$ compatibility condition

In this section we derive a compatibility condition for the system (2.13), the result of which is an equation posed on the long-scale, which governs the decaying envelope function in the cladding layers. The method is analogous to that used in section B; we begin by dividing the first line of (2.13) by k_i^2, so we have in each layer:

$$\frac{1}{k_i^2}H_{2,\xi\xi}+H_2=-\frac{1}{k_i^2}\Big(2H_{1,R\xi}+\frac{1}{R}H_{1,\xi}+H_{0,RR}+\frac{1}{R}H_{0,R}-\frac{\xi}{R^2}H_{0,\xi}-\frac{m^2}{R^2}H_0+n_i^2\Omega_2^2H_0\Big). \tag{C.1}$$

Following an analogous approach to that of the previous section, we can show that

$$\begin{aligned}0=&\left[\frac{1}{k_i^2}(H_{1,R}+H_{2,\xi})h_0\right]_{0^+,-1}^{0^-,\,\alpha}+\left[\frac{1}{k_i^2}H_{1,R}h_0\right]_{0^+,-1}^{0^-,\,\alpha}\\&+\int_{-1}^{\alpha}\frac{1}{k_i^2}\Big(-2H_{1,R}h_{0,\xi}+\frac{1}{R}H_{1,\xi}h_0+H_{0,RR}h_0\\&\qquad+\frac{1}{R}H_{0,R}h_0-\frac{\xi}{R^2}H_{0,\xi}h_0-\frac{m^2}{R^2}H_0h_0+n_i^2\Omega_2^2H_0h_0\Big)\mathrm{d}\xi.\end{aligned} \tag{C.2}$$

Using the boundary conditions (2.14), we can substitute the terms in the first square bracket to get

$$\begin{aligned}0=&\left[\frac{1}{k_i^2}\left(\frac{\beta m}{i\mu_i\Omega_0}\frac{E_1}{R}+\Omega_2^2\Big(\frac{1}{k_i^2}-\frac{1}{2\Omega_0^2}\Big)H_{0,\xi}\right)h_0\right]_{0^+,-1}^{0^-,\,\alpha}+\left[\frac{1}{k_i^2}H_{1,R}h_0\right]_{0^+,-1}^{0^-,\,\alpha}\\&-\int_{-1}^{\alpha}\frac{1}{k_i^2}\Big(-2H_{1,R}h_{0,\xi}+\frac{1}{R}H_{1,\xi}h_0+H_{0,RR}h_0\\&\qquad+\frac{1}{R}H_{0,R}h_0-\frac{\xi}{R^2}H_{0,\xi}h_0-\frac{m^2}{R^2}H_0h_0+n_i^2\Omega_2^2H_0h_0\Big)\mathrm{d}\xi.\end{aligned} \tag{C.3}$$

Finally, we substitute in the separated-scale expressions for the various field components, yielding the long-scale equation (2.16):

$$f_{0,RR}+\frac{c_1}{R}f_{0,R}+\left(\Omega_2^2c_2^2-\frac{c_3^2}{R^2}\right)f_0=0, \tag{C.4}$$

where $c_1=\tilde{c}_1/P$, $c_2^2=\tilde{c}_2^2/P$, $c_3^2=\tilde{c}_3^2/P$, and

$$
\begin{aligned}
\tilde{c}_1 &= \left[-\frac{1}{k_i^2}\hat{h}_1 h_0 \right]_{0^+,-1}^{0^-,\,\alpha} + \int_{-1}^{\alpha} \frac{1}{k_i^2}\left(-2h_{0,\xi}\hat{h}_1 + h_{1,\xi}h_0 + |h_0|^2\right) \mathrm{d}\xi, \\
\tilde{c}_2^2 &= \left[-\frac{1}{k_i^4}h_{0,\xi}h_0 \right]_{0^+,-1}^{0^-,\,\alpha} + \int_{-1}^{\alpha} \frac{1}{k_i^2} n_i^2 |h_0|^2 \mathrm{d}\xi, \\
\tilde{c}_3^2 &= \left[\frac{1}{k_i^2}\left(\frac{\beta m}{i\mu_i \Omega_0}\hat{e}_1 h_0 - \hat{h}_1 h_0 \right) \right]_{0^+,-1}^{0^-,\,\alpha} + \int_{-1}^{\alpha} \frac{1}{k_i^2}\left(-2h_{0,\xi}\hat{h}_1 - \hat{h}_{1,\xi}h_0 + \xi h_{0,\xi}h_0 + m^2|h_0|^2\right) \mathrm{d}\xi, \\
P &= \left[-\frac{1}{k_i^2}h_1 h_0 \right]_{0^+,-1}^{0^-,\,\alpha} + \int_{-1}^{\alpha} \frac{1}{k_i^2}\left(-2h_{0,\xi}h_1 + |h_0|^2\right) \mathrm{d}\xi.
\end{aligned}
\tag{C.5}
$$

D. Explicit solutions for TE-dominated modes

For TE-dominated modes, the standing-wave solution to (2.7) is given by $H_0 = f_0(R)h_0(\xi)$, $E_0 \equiv 0$, where

$$
h_0(\xi) = \begin{cases} A\cos(k_1\xi) + B\sin(k_1\xi), & \xi \in [-1,0], \\ C\cos(k_2\xi) + D\sin(k_2\xi), & \xi \in [0,\alpha]. \end{cases}
\tag{D.1}
$$

The coefficients are given (up to a constant normalisation factor) by

$$
\begin{aligned}
A &= k_1\mu_2\sin(k_1) - k_2\mu_1\sin(k_2\alpha), \qquad B = k_1\mu_2(\cos(k_1) + \cos(k_2\alpha)), \\
C &= k_1\mu_2\sin(k_1) - k_2\mu_1\sin(k_2\alpha), \qquad D = k_2\mu_1(\cos(k_1) + \cos(k_2\alpha)),
\end{aligned}
\tag{D.2}
$$

and equation (2.9) is used to find Ω_0.

At $O(\eta)$ we find the solution to (2.10) is given by $H_1 = f_0(R)\hat{h}_1(\xi)/R + f_{0,R}(R)h_1(\xi)$, where

$$
\hat{h}_1(\xi) = \begin{cases} A'\cos(k_1\xi) + B'\sin(k_1\xi) - \frac{1}{2}A\xi\cos(k_1\xi) - \frac{1}{2}B\xi\sin(k_1\xi), \xi \in [-1,0], \\ C'\cos(k_2\xi) + D'\sin(k_2\xi) - \frac{1}{2}C\xi\cos(k_1\xi) - \frac{1}{2}D\xi\sin(k_1\xi), \xi \in [0,\alpha], \end{cases}
\tag{D.3}
$$

with

$$
\begin{aligned}
A' &= \frac{1}{2}(k_1\mu_2\sin(k_1) + k_2\mu_1\sin(k_2\alpha)), \\
B' &= \frac{1}{2k_1k_2}\left(k_1^2k_2\mu_2\cos(k_1) - k_1^2k_2\mu_2\cos(k_2\alpha) + k_1^2\mu_2\sin(k_2\alpha) - k_2^2\mu_1\sin(k_2\alpha)\right) \\
C' &= \frac{1}{2}(k_1\mu_2\sin(k_1) + k_2\mu_1\sin(k_2\alpha)), \\
D' &= \frac{1}{2k_1k_2}\left(k_1k_2^2\mu_1\cos(k_1) - k_1k_2^2\mu_1\cos(k_2\alpha) + k_1^2\mu_2\sin(k_1) - k_2^2\mu_1\sin(k_1)\right),
\end{aligned}
\tag{D.4}
$$

and

$$h_1(\xi) = \begin{cases} A'' \cos(k_1\xi) + B'' \sin(k_1\xi) - A\xi\cos(k_1\xi) - B\xi\sin(k_1\xi), \xi \in [-1,0], \\ C'' \cos(k_2\xi) + D'' \sin(k_2\xi) - C\xi\cos(k_1\xi) - D\xi\sin(k_1\xi), \xi \in [0,\alpha], \end{cases} \tag{D.5}$$

with

$$\begin{aligned} A'' &= k_1\mu_2\sin(k_1) + k_2\mu_1\sin(k_2\alpha), \qquad B'' = k_1\mu_2(\cos(k_1) - \cos(k_2\alpha)), \\ C'' &= k_1\mu_2\sin(k_1) + k_2\mu_1\sin(k_2\alpha), \qquad D'' = k_2\mu_1(\cos(k_1) - \cos(k_2\alpha)). \end{aligned} \tag{D.6}$$

The electric field component at this order is generally non-zero and given by $E_1 = f_0(R)\hat{e}_1(\xi)/R$, where

$$\hat{e}_1(\xi) = \begin{cases} A''' \cos(k_1\xi) + B''' \sin(k_1\xi), & \xi \in [-1,0], \\ C''' \cos(k_2\xi) + D''' \sin(k_2\xi), & \xi \in [0,\alpha]. \end{cases} \tag{D.7}$$

The coefficients in the above solution are readily found using the boundary conditions in (2.12) along with the preceding solutions in this section, but their closed form is complicated and not suitable for publication.